# 锌对 SnxZn/Cu 界面微空洞的影响

杨 扬[1], 陆 皓[1,2], 余 春[1], 陈俊梅[1], 陈振英[1]
(1. 上海交通大学 材料科学与工程学院, 上海 200240;
2. 上海交通大学 激光制造与材料改性上海市重点实验室, 上海 200240)

**摘 要:** 通过向锡钎料中添加不同含量的 Zn 元素,系统研究了锌对 Sn$x$Zn/Cu($x$ = 0, 0.2, 0.5, 0.8 (质量分数,%)) 界面处柯肯达尔空洞形成的影响. 结果表明,经热老化处理后,纯 Sn/Cu 接头中的 $Cu_3Sn$ 层和 $Cu_3Sn$/Cu 界面出现了大量柯肯达尔空洞. 然而随着 Zn 元素含量的增加,反应界面处的 $Cu_3Sn$ 层逐渐变薄甚至消失,柯肯达尔空洞也随之显著减少或消失; 锌在反应界面处的富集现象越来越显著. 锌参与了界面反应,形成了 $(Cu,Zn)_6Sn_5$ 相、$Cu_6(Sn,Zn)_5$ 相和 Cu-Zn 固溶合金,其中 Cu-Zn 固溶合金层可以显著影响铜的界面扩散. Zn 元素直接参与了界面扩散,在很大程度上缓和铜和锡的不平衡扩散,从而有效抑制了柯肯达尔空洞的形成.

**关键词:** 锌; 界面; 柯肯达尔空洞; 金属间化合物
**中图分类号:** TG146.23 **文献标识码:** A **文章编号:** 0253-360X(2013)01-0053-04


杨 扬

## 0 序 言

随着电子产品的微型化和多功能化,电子封装的密度不断增加,焊点(钎焊接头)的尺寸越来越小,使得反应界面占整个接头的比例越来越大. 因此界面微观组织对接头可靠性的影响也越来越大. 在固态热老化处理的过程中,接头的反应界面处常会出现密度较高的柯肯达尔空洞(kirkendall void),其对接头可靠性的影响不容忽视[1-4]. 故此如何抑制或消除界面柯肯达尔空洞已成为国内外学术界的一个新的关注点.

在锡基钎料/铜界面处,柯肯达尔空洞与 $Cu_3Sn$ 层存在很强的关联性,前者常随着后者的形成而出现,并随着后者的减薄而减少或消失. 近年来,研究者们常利用这个规律,通过向钎料内添加合金元素,阻缓 $Cu_3Sn$ 层的生长,从而抑制柯肯达尔空洞的形成. 研究结果表明,Zn 元素对界面柯肯达尔空洞的抑制效果较为显著[5-7]. 尽管与锌合金化相关的研究工作很多,但是对于究竟向钎料中添加多少锌能够显著地抑制空洞的形成还不得而知.

基于此文中通过向纯锡钎料中添加不同含量的锌,以系统地研究其对 Sn/Cu 界面处柯肯达尔空洞形成的影响,并初步探讨了锌对空洞的抑制机理.

## 1 试验方法

Sn$x$Zn($x$ = 0.2, 0.5, 0.8 (质量分数,%)) 钎料由锡粒和锌粒(纯度均为 99.9%) 炼制而成. 基板的制备工艺为在铜箔(纯度为 99.9%; 厚度为 0.1 mm) 表面电镀一层厚度约为 10 μm 的铜膜,然后将其剪切成尺度为 10 mm × 10 mm 的小片. 为除去表面氧化层及油污,将箔片依次用质量分数为 5% 的 NaOH 和体积分数为 5% 的 HCl 溶液清洗,每步清洗之后需用去离子水冲洗. 将重约 200 mg 的钎料置于箔片中心,并在表面涂覆助焊剂,接着将它们放入加热炉内进行 260 ℃回流处理. 然后对焊态样品在 180 ℃分别进行 3, 7 d 的时间固态热老化处理.

热老化试样制备完毕后,采用环氧树脂及固化剂将其冷镶,并对其截面进行研磨和抛光处理. 之后利用扫描电子显微镜(SEM) 中的背散射电子成像技术(BSE) 对试样反应界面的微观组织形貌进行表征,采用能谱仪(EDX) 进行成分分析.

## 2 试验结果及分析

图 1a 为回流态未经热老化处理的 Sn/Cu 界面的微观组织形貌,界面处形成一薄层扇贝形

收稿日期: 2011-11-22
基金项目: 国家自然科学基金资助项目(50975176, 51105251)

$Cu_6Sn_5$，没有柯肯达尔空洞出现. 回流态接头经 180 ℃热老化处理 72 h 后，在 $Cu_3Sn$ 层和 $Cu_3Sn$/Cu 界面处就发现了高密度的柯肯达尔空洞，如图 1b 所示. 并且越靠近铜基板，空洞密度越高.

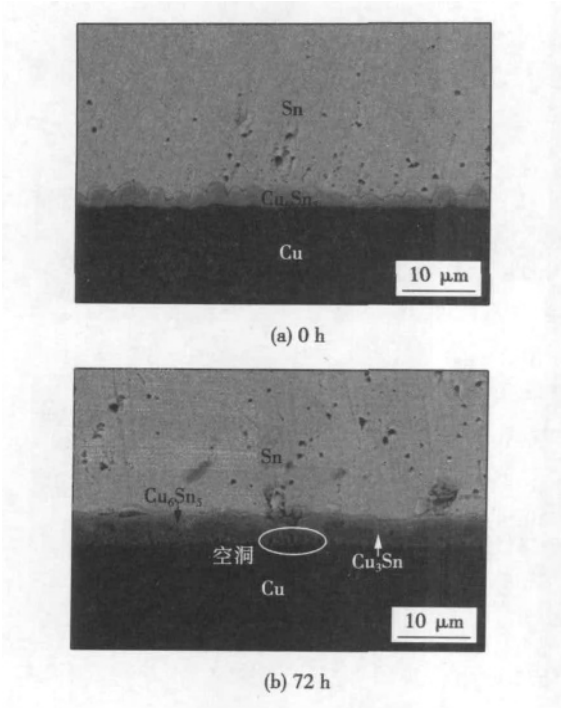


图 1 经 180 ℃热老化处理的 Sn/Cu 界面的微观组织形貌

Fig. 1 Interfacial microstructure of Sn/Cu joints after aging at 180 ℃

与回流态 Sn/Cu 接头中的界面组织形貌相似（图 1a），Sn$x$Zn/Cu（$x$ = 0.2，0.5，0.8（质量分数，%））界面处也均形成了扇贝形 $Cu_6Sn_5$ 层，且没有柯肯达尔空洞出现（由于形貌类似，文中没有赘加相关的 SEM 图片）.

图 2 和图 3 分别为 Sn$x$Zn/Cu 接头经 180 ℃热老化处理 72 h 和 168 h 后的界面微观组织形貌. 经热老化处理 72 h 后，Sn0.2Zn/Cu 界面处形成了连续的 $Cu_6Sn_5$ 和 $Cu_3Sn$ 层，$Cu_3Sn$ 层的厚度较小（0.69 μm），约为 $Cu_6Sn_5$ 层厚度的 1/2；在 $Cu_3Sn$ 薄层中出现了少量的柯肯达尔空洞. 在 Sn0.5Zn/Cu 接头中，界面处也出现了较厚的 $Cu_6Sn_5$ 层，但 $Cu_3Sn$ 层变得更薄，约为 0.34 μm，如图 2b 所示. 当 Zn 元素含量增至 0.8% 时，界面处仅存在 $Cu_6Sn_5$ 层，很难观察到 $Cu_3Sn$ 相，如图 2c 所示. 在后两种 Zn 元素含量较高接头的 SEM 图片中，已很难分辨空洞的存在.

热老化时间延长至 168 h 后，Sn0.2Zn/Cu 界面处形成了不连续的 $Cu_3Sn$ 层，层内柯肯达尔空洞的数量很少，如图3a所示；在Sn0.5Zn/Cu界面处，

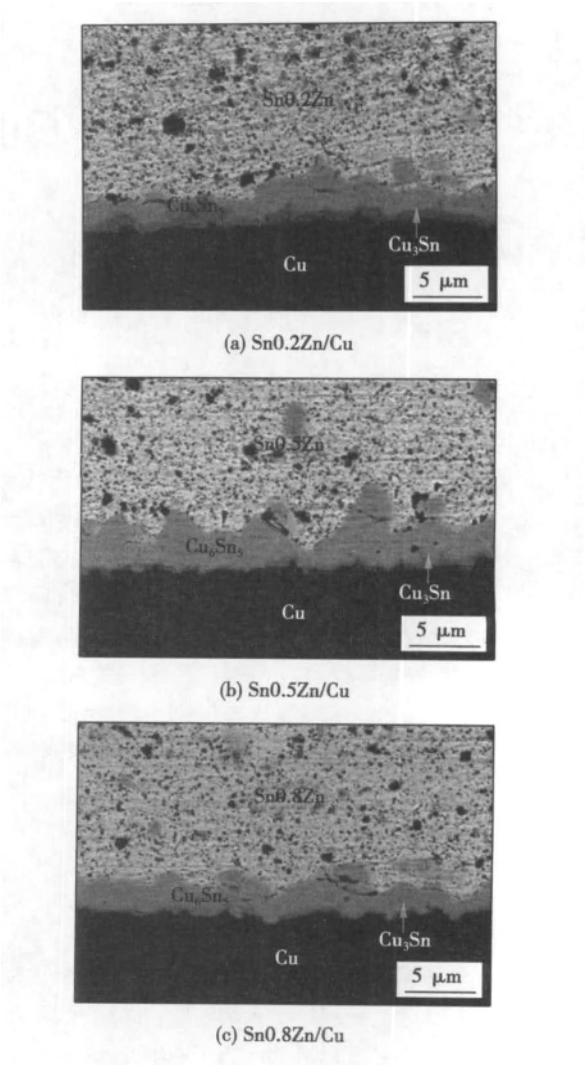


图 2 经 180 ℃热老化处理 72 h 的 Sn$x$Zn/Cu 界面的微观组织形貌

Fig. 2 Interfacial microstructure of Sn$x$Zn/Cu joints after aging at 180 ℃ for 72 h

$Cu_3Sn$ 层的厚度没有明显变化，如图 3b 所示；而在 Sn0.8Zn/Cu 界面处，$Cu_3Sn$ 相完全消失，同时另一种金属间化合物（IMC）层在 $Cu_6Sn_5$ 层上部形成，如图 3c 所示. 在后两种接头的界面处也没有发现空洞.

由试验结果可以发现，Zn 元素的含量对界面处 $Cu_3Sn$ 层的厚度影响很大. 随着锡钎料中 Zn 元素含量的增加，$Cu_3Sn$ 层的厚度逐渐减少，甚至在 Sn0.8Zn/Cu 接头中观察不到 $Cu_3Sn$ 相. 随着 $Cu_3Sn$ 层的减少和消失，柯肯达尔空洞的形核生长也被有效地抑制. 此外 $Cu_3Sn$ 相的 Cu 元素含量明显高于 $Cu_6Sn_5$ 相，故 $Cu_3Sn$ 相的减少意味着锌对界面处铜扩散的抑制效果较为显著.

为进一步研究 Zn 元素对界面处空洞形成和组分元素扩散的影响，文中采用能谱仪对Sn$x$Zn/Cu

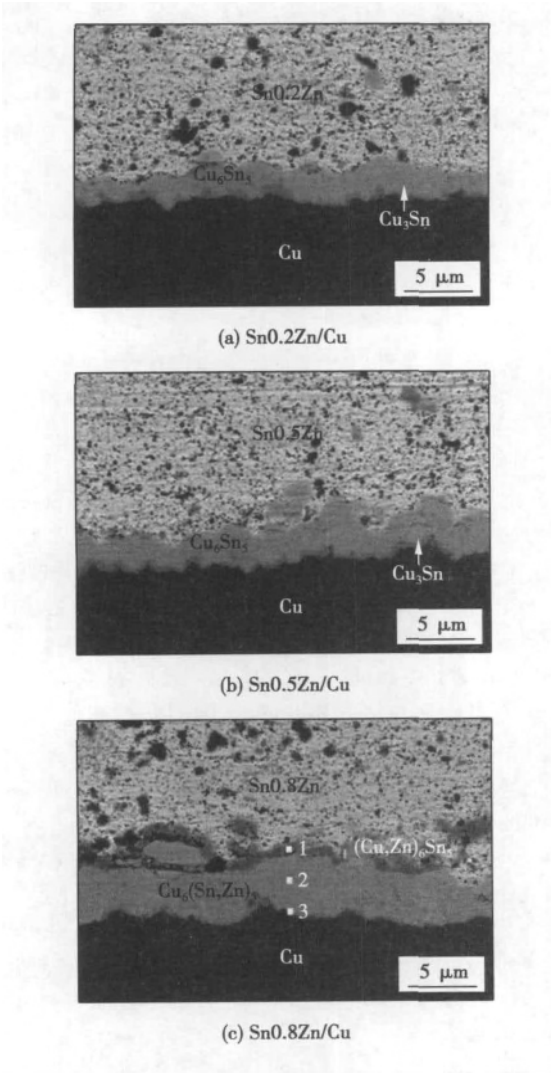


**图 3　经 180 ℃热老化处理 168 h 的 Sn$x$Zn/Cu 界面的微观组织形貌**

Fig. 3　Interfacial microstructure of Sn$x$Zn/Cu joints after aging at 180 ℃ for 168 h

界面进行了成分分析. 经 180 ℃热老化处理 168 h 的 Sn0.2Zn/Cu 界面的能谱(线扫描)分析结果表明,Zn 元素的分布比较均匀,没有明显的富集现象; 而对于相同处理条件下的 Sn0.5Zn/Cu 接头中, $Cu_6Sn_5$/Cu 界面处 Zn 元素的含量较高,有富集趋势. 图 4 为 Sn0.8Zn/Cu 界面的能谱分析结果. 在回流态界面处,Zn 元素的分布也比较均匀. 经热老化处理 168 h 后,Sn0.8Zn/$Cu_6Sn_5$ 和 $Cu_6Sn_5$/Cu 界面均产生了明显的锌富集现象,前者界面处的 Zn 元素的含量高于后者界面. 所有含锌接头中, Sn0.8Zn/Cu 界面处的 Zn 元素的含量最高,而其回流态界面没有出现锌富集现象. 这表明在 Sn$x$Zn/Cu 接头的回流过程中,液态钎料中的锌向反应界面扩散的动力较小; 在 Zn 元素的含量低于 0.8% 界面处,均没有锌富集现象. 在热老化过程中,固态钎料基体中的锌开始向 Sn$x$Zn/IMC 界面扩散,并逐渐形成富集. 随着 Zn 元素含量的增加,这一现象越来越显著. 在 Zn 元素含量较低的接头中,由于界面处锌的浓度梯度较低,其主要在 Sn$x$Zn/Cu 界面富集,而不易扩散通过 IMC 层; 而对于 Zn 元素含量较高的接头锌的扩散动力很大,其不仅在 Sn0.8Zn/$Cu_6Sn_5$ 界面产生富集,而且可以通过 $Cu_6Sn_5$ 层扩散,在 $Cu_6Sn_5$/Cu 界面也产生富集.

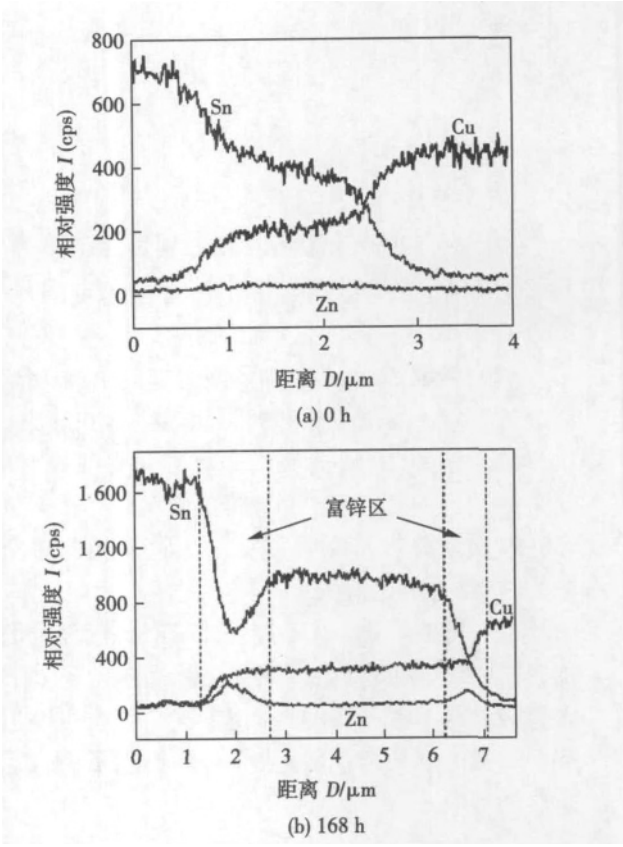


**图 4　经 180 ℃热老化处理的 Sn0.8Zn/Cu 界面的成分分布**

Fig. 4　EDX analysis of Sn0.8Zn/Cu interface after aging at 180 ℃

在图 4b 中,锌的分布呈现为两端区域高而中间区域低的趋势,这说明界面处可能存在 3 个 IMC 层. 故此文中对 Sn0.8Zn/Cu 界面处的 IMC 层区域(图 3c)进行了点扫描分析. 结果表明,界面主要由 3 个层组成,灰色 IMC 层(2 点)的成分为铜(原子分数 54.62%)、锌(原子分数 5.26%)和锡(原子分数 40.12%),按比例可将其表征为 $Cu_6(Sn,Zn)_5$; $Cu_6(Sn,Zn)_5$层上方的黑色相(1 点)的成分为铜(原子分数 33.15%)、锌(原子分数 20.27%)和锡(原子分数为 46.58%),将其判定为$(Cu,Zn)_6Sn_5$; $Cu_6(Sn,Zn)_5$ 层下方靠近基板一侧(3 点)的成分为铜(原子分数为 61.70%)、锌(原子分数为 25.32%)和锡(原子分数为 12.98%),该富锌层为 Cu-Zn 固

溶合金[6].

在 Sn$x$Zn/Cu 接头的界面反应过程中，Zn 元素直接参与了铜和锡的互扩散，并对它们的扩散产生了很大影响. 界面互扩散由二元扩散

$$J_v + J_{Cu} + J_{Sn} = 0 \quad (1)$$

转变为三元扩散

$$J_v + J_{Cu} + J_{Sn} + J_{Zn} = 0 \quad (2)$$

式中：$J_v$ 为所研究区域内空位的扩散通量；$J_{Cu}$，$J_{Sn}$和 $J_{Zn}$分别为铜、锡和锌的扩散通量. 锌与锡的扩散方向一致，其可以在很大程度上缓和铜和锡的不平衡扩散，从而有效抑制了空洞的形成.

## 3 结 论

(1) Sn/Cu 接头经热老化处理后，在 $Cu_3Sn$ 层和 $Cu_3Sn$/Cu 界面出现了许多柯肯达尔空洞，且越靠近 $Cu_3Sn$/Cu 界面，空洞密度越高.

(2) 微量 Zn 元素的加入显著抑制了 Sn$x$Zn/Cu 界面处 $Cu_3Sn$ 层的生长和柯肯达尔空洞的形成. 当 Zn 元素含量为 0.5%(质量分数)时，界面处 $Cu_3Sn$ 层很薄，层中存在极少量空洞；而 Zn 元素含量为 0.8%(质量分数)时，界面处的 $Cu_3Sn$ 相几乎全部消失，空洞也随之消失.

(3) 随着 Sn$x$Zn/Cu 接头中 Zn 元素含量的增加，锌在反应界面处的富集现象越来越显著. Zn 元素直接参与了铜和锡的界面扩散，在很大程度上缓和铜和锡的不平衡扩散，从而有效抑制了柯肯达尔空洞的形成.

(4) Zn 元素的添加改变了反应界面的微观组织，形成了 3 个分层，依次为 $(Cu,Zn)_6Sn_5$ 层、$Cu_6(Sn,Zn)_5$ 层和 Cu-Zn 固溶合金层. 其中 Cu-Zn 固溶合金层影响了界面 Cu 元素的扩散.

## 参考文献：


[1] Anderson I E, Harringa J L. Elevated temperature aging of solder joints based on Sn-Ag-Cu: Effects on joint microstructure and shear strength [J]. Journal of Electronic Materials, 2004, 33(12): 1485 - 1496.

[2] Zeng K, Stierman R, Chui T, *et al*. Kirkendall void formation in eutectic SnPb solder joint on bare Cu and its effect on joint [J]. Journal of Applied Physics, 2005, 97(2): 024508.

[3] Mattila T, Kivilahti J. Reliability of lead-free interconnections under consecutive thermal and mechanical loadings [J]. Journal of Electronic Materials, 2006, 35(2): 250 - 256.

[4] Xu L, Pang J, Che F. Impact of thermal cycling on Sn-Ag-Cu solder joints and board-level reliability [J]. Journal of Electronic Materials, 2008, 37(6): 880 - 886.

[5] Anderson I E, Harringa J L. Suppression of void coalescence in thermal aging of tin-silver-copper-X solder joints [J]. Journal of Electronic Materials, 2006, 35(1): 94 - 106.

[6] Cho M G, Kang S K, Shih D Y, *et al*. Effects of minor additions of Zn on interfacial reactions of Sn-Ag-Cu and Sn-Cu Solders with various Cu substrates during thermal aging [J]. Journal of Electronic Materials, 2007, 36(11): 1501 - 1509.

[7] Kim J Y, Yu J, Kim S H. Effects of sulfide-forming element additions on the Kirkendall void formation and drop impact reliability of Cu/Sn-3.5Ag solder joints [J]. Acta Materialia, 2009, 57(17): 5001 - 5012.



**作者简介：** 杨 扬，男，1982 年出生，博士研究生. 主要从事钎焊微连接方面的科研工作. 发表论文 10 余篇. Email: yy198283@126.com

**通讯作者：** 陆 皓，男，教授，博士研究生导师. Email: shweld@sjtu.edu.cn

indicates that the flow behavior of filler metal in unparalleled clearance is influenced by the combined effect of ultrasonic induced gap-filling action and capillary action.

**Key words:** ultrasonic brazing; high-speed video camera investigation; gap; filling gap; dynamics

**Effect of pre-oxidation treatment on thermal shock resistance and residual stress of thermal barrier coating** LI Yajuan[1], DONG Yun[2], WANG Zhiping[1], LIU Shiqiang[3] (1. College of Science, Civil Aviation University of China, Tianjin 300300, China; 2. Department of Materials Science and Engineering, Northeastern University at Qinhuangdao, Qinhuangdao 066004, China; 3. School of Materials Science and Engineering, Hebei University of Technology, Tianjin 300130, China). pp 37 - 40

**Abstract:** The thermal barrier coating by taking MCrAlY as bonding coating and $ZrO_2 + 8\% Y_2O_3$ as top coating were deposited on the nickel-based super-alloy by air plasma spraying. Pre-oxidation treatment was carried out on the thermal barrier coatings by controlling the oxygen pressure in high vacuum sintering furnace. Then, the effects of pre-oxidation treatment on the thermal shock resistance and residual stress were investigated, respectively. The results show that pre-oxidation treatment improves the density of bonding coating, which makes it uniform and reduces the probability of complex stress caused by convex point in interface area. Meanwhile, pre-oxidation treatment interferes the growth process of thermally grown oxide (TGO), reduces the TGO growth rate and the stress concentration of coating. Residual stress increases with the increasing of thermal cycles. However, pre-oxidation treatment can slow down the increasing rate of residual stress. The residual stress of 650.1 MPa can be reached after 350 thermal cycles without pre-oxidation, while the residual stress is only 492.5 MPa after 400 thermal cycles with pre-oxidation.

**Key words:** pre-oxidation treatment; thermal barrier coating; thermally grown oxide; residual stress

**Calibration of relative position and orientation between robot and positioner based on spheres fitting method** ZHU Xiaopeng, ZHANG Ke, TU Zhiqiang, HUANG Jie (Shanghai Key Laboratory of Laser Manufacturing & Material Modification, Shanghai Jiao Tong University, Shanghai 200240). pp 41 - 44

**Abstract:** A method to calibrate the relative position and orientation between robot and positioner was presented by fitting sphere based on the least square method. Firstly, the positioner rotates or tilts to different positions, and the position data of TCP were recorded in the same time. The optimal sphere was fitted by the least square method, and the origin of base coordinate frame of the positioner was calculated. Secondly, several points were recorded in the same way to calculate the vectors of axis. In order to avoid the effects of causal factors, the concept of deviation rate was presented to verify the accuracy of the marked points. Experiments show that this method can reduce the random error and avoid the effects of causal factors, which has high precision.

**Key words:** robot; laser cladding; calibration; sphere fitting method; least square method

**Spectrum of MIG arc at different welding parameters** LI Zhiyong, ZHANG Wenzhao, LI Yan, DING Jingbin (Welding Research Center, North University of China, Taiyuan 030051, China). pp 45 - 48, 52

**Abstract:** The droplet transfer mode and arc length variation are the significant factors affecting the radiation intensity of arc plasma for MIG welding. It is critical to understand the regularity of the radiation fluctuation in application in industry control of the welding process. Therefore, the spectrum of MIG arc radiation was collected with a spectrometer based system. The spectrums of welding processes at different welding parameters were analyzed to study the regularity of the radiation variation. Based on the arc physics, the spectral information combining with the droplet transfer mode was used to get a better understanding of the arc radiation. The results show that the arc spectrum with its distinct distribution is different at different welding parameters. The MIG arc emits wavy radiation due to droplet transfer. The spectral signals in different spectrum bands, such as ultraviolet, visible and near infrared band, have totally different variation characteristics during different instance of the droplet transfer.

**Key words:** arc spectrum; welding parameter; MIG welding; droplet transfer

**Microstructure and properties of diffusion bonded interface of titanium-copper interlayer-carbon steel composite tube** LIU Deyi, CAI Jianwei, REN Ruiming (School of Materials Science and Engineering, Dalian Jiaotong University, Dalian 116028, China). pp 49 - 52

**Abstract:** The composite tube of titanium/steel was prepared by the drawing and inner pressure diffusion technique by using Cu foil as an interlayer. The interface microstructure, fractured surface and components were investigated with OM, SEM, XRD and EDS. The bonding strength of the interface was studied by shear test. The results show that the metallurgical bonding of titanium and steel was obtained by the drawing and inner pressure diffusion technique with copper foil as an interlayer. The interface components analysis show that the elements diffusion was found between the titanium/copper interface and the diffusion layer was formed. The thickness of the diffusion layer increased with increasing of diffusing time. The Fe-Ti brittle compound was prevented by using copper interlayer at lower diffusion temperature. The shear strength of titanium/steel interface firstly increased and then decreased with diffusion temperature increasing. Copper interlayer can improve the shear strength significantly, and the maximum shear strength can reach 310 MPa.

**Key words:** titanium/steel; interlayer; diffusion bonding; bonding strength

**Effect of Zn on formation of voids on Sn*x*Zn/Cu interface** YANG Yang[1], LU Hao[1,2], YU Chun[1], CHEN Junmei[1], CHEN Zhenying[1] (1. School of Materials Science and Engineering, Shanghai Jiaotong University, Shanghai 200240, China; 2. Key Laboratory of Shanghai Laser Manufacturing and Materials Modification, Shanghai Jiaotong University, Shanghai 200240, China). pp 53 - 56

**Abstract:** The effect of Zn on formation of Kirkendall voids on the interface was studied through the reaction between Sn*x*Zn solders ($x = 0, 0.2\%, 0.5\%, 0.8\%$) and the electroplated Cu substrate. During the thermal aging of Sn/Cu joints, a number of Kirkendall voids were formed in the $Cu_3Sn$ layer and on the $Cu_3Sn$/EPC interface. With the increase of Zn content in solder, the growth of $Cu_3Sn$ layer was greatly suppressed, and the formation of Kirkendall voids was effectively inhibited. The concentration of Zn on the reaction interface also significantly increased. Zn participated in the interface reaction, (Cu,

Zn)$_6$Sn$_5$, Cu$_6$(Sn, Zn)$_5$ and Cu-Zn solid-solution alloy were formed, among which the Cu-Zn solid-solution alloy layer can greatly affect the diffusion of Cu. Zn served as a diffusing element during the interface reaction, which can improve the unbalanced diffusion of Cu and Sn to a great degree, and suppress the formation of voids effectively.

**Key words:** Zn; interface; Kirkendall void; intermetallic compound

**Stress analysis of plain dent on pipeline based on finite element method** WU Ying[1], ZHANG Peng[1], XIE Yanping[2] (1. School of Civil Engineering and Architecture, Southwest Petroleum University, Chengdu 610500, China; 2. Oil and Gas Production Capacity Construction Project, Department of PetroChina Tarim Oilfield, Korla 841000, China). pp 57 – 60

**Abstract:** For the typical plain dent on pipeline, according to the actual operation situation of the pipeline, the finite element models were established. When other parameters were invariable, a large number of calculations were carried out by changing dent depth, pipe wall thickness, pipe diameter and longitudinal dent length. The calculation results were sorted, inducted, and plotted. On this basis, the results were analyzed by single factor and multiple factors analysis, and then the changing rules between the stress and various parameters were obtained. Non-linear regression analysis was utilized to fit the results. The results show that the relationships between the maximum stress in the dented pipeline, the dent depth, wall thickness, diameter of pipeline, and the longitudinal length of the dent were modeled by sine, index, linear and semi-log liner function, respectively. Some specific expression are obtained in certain range.

**Key words:** pipeline; plain dent; stress; finite element method; fitting

**Study on humping bead formation mechanism in thick-wire high-speed MAG welding** YANG Zhanli, ZHANG Shanbao, YANG Yongbo, TANG Qilong* (Harbin Welding Institute, China Academy of Machinery Science & Technology, Harbin 150080, China). pp 61 – 64

**Abstract:** The humping bead formation mechanism in the thick-wire($\phi$ 3.2) high-speed MAG welding process was studied. Using the high-speed camera system, the arc shape and weld pool flow were investigated. By analyzing the captured image, the viewpoint of dynamic equilibrium point was presented. The distance between the dynamic equilibrium point and the arc is the cause of humping bead formation. Any factors to prompt the dynamic equilibrium point to move to the arc, will prevent formation of humping bead. In contrast, any factors to prompt the dynamic equilibrium point away from the arc, will lead to the appearance of humping bead. Furthermore, the uphill and downhill welding experiments were designed to verify the correctness of the above discussion about humping bead formation mechanism.

**Key words:** humping bead; undercut; molten pool; high speed camera system

**Continuous trajectory model of intersecting joint welding robot based on groove feature** WANG Tianqi, LI Liangyu, YUE Jianfeng (Tianjin Key Laboratory of Modern Electromechanical Equipment Technology, Tianjin Polytechnic University, Tianjin 300387, China). pp 65 – 68

**Abstract:** A continuous trajectory mathematical model was established for offshore platform jacket welding robot. The robot with 5 degrees of freedom has enough workspace to finish automatic welding of Y joint and flexibility to meet the requirement for obstacle avoidance in K-joint welding. The kinematics of the robot was built according to the robot structure. Since this robot has a redundant degree of freedom, the joint value was calculated by two steps methods. To ensure the motion stability of the robot, the joint velocity was calculated by derivation operation of joint value through limited method. The simulation result shows that this robot can achieve automatic welding of the K, Y, T joint, and the mathematical model of joint value and velocity can be used to control this robot.

**Key words:** pipe joint with groove feature; multi-pass welding; offshore platform jacket

**Design of human-machine interactive robotic arc welding remanufacturing system** YIN Ziqiang[1,2], ZHANG Guangjun[2], ZHAO Huihui[2], YUAN Xin[1], WU Lin[2] (1. Institute of Oceanographic Instrumentation, Shandong Academy of Sciences, Qingdao 266001, China; 2. State Key Laboratory of Advanced Welding and Joining, Harbin Institute of Technology, Harbin 150001, China). pp 69 – 72

**Abstract:** On the basis of analyzing the characters of the worn parts, a novel remanufacturing solution was proposed. The remanufacturing of the worn parts was realized by a human-machine interactive remanufacturing system based on robotic GMAW. The system takes operators as the intelligent factor to solve the complicated problems of the system, which are nonlinear and hard to model. The computer and machine were employed to solve the high speed and high accuracy problem, for instance the numerical computation and motion control etc. After the experiment system platform being established, the structure of the system software and the human-machine interactive scheme were studied, and the visual human-machine interface was designed by modularized program.

**Key words:** human-machine interactive; robotic arc welding; remanufacturing; off-line programming

**Influence of joint geometric parameters on stress concentration factor for under-matched butt joint under three-point bending load** WANG Jiajie[1,2], DONG Zhibo[1], ZHANG Jingqiang[1], LIU Xuesong[1], FANG Hong yuan[1*] (1. State Key Laboratory of Advanced Welding and Joining, Harbin Institute of Technology, Harbin 150001, China 2. School of Materials and Chemical Engineering, Heilongjiang Institute of Technology, Harbin 150050, China). pp 73 – 76

**Abstract:** In order to improve the bending load-carrying capacity (BLCC) for under-matched butt joints in the elastic stage, the influence of joint geometric parameters on bending stress concentration factor (BSCF) for under-matched butt joint with X-type groove and double side symmetrical type reinforcement was studied based on the finite element method from the viewpoint of materials mechanics. The influence rules of joint geometric parameters on BSCF at the geometric mutations area near fusion line and in the weld bottom center show that the reinforcement plays the most important role in BSCF, the cover pass width has relatively great effect on BSCF and the weld toe radius has